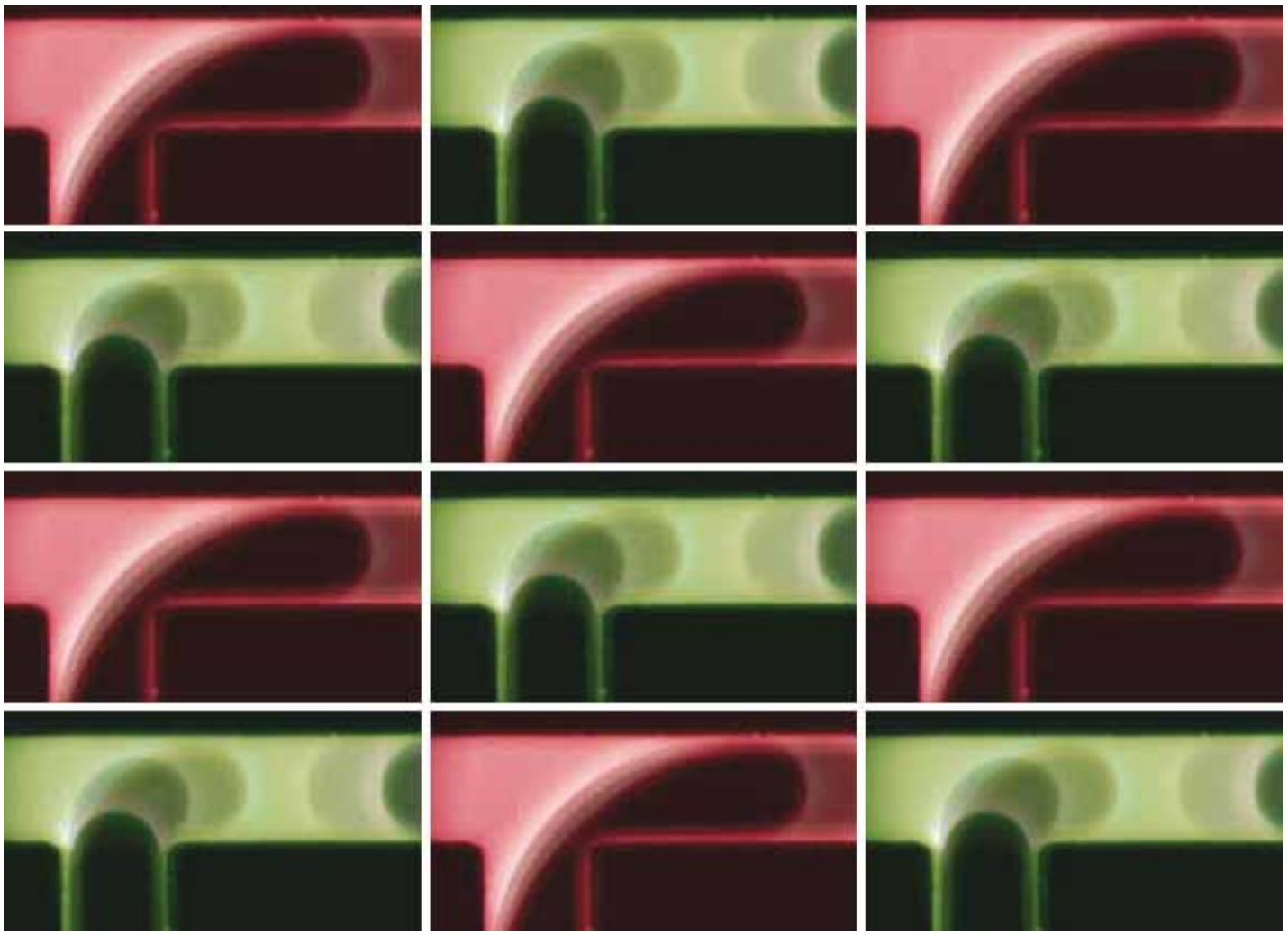

Featuring work from the groups of Professor Kleijn and Professor Kreutzer at Delft University of Technology, the Netherlands.

Title: Predictive model for the size of bubbles and droplets created in microfluidic T-junctions

The size of bubbles and droplets strongly depends on the shape of the junction in which they form and can be predicted from first principles.

As featured in:

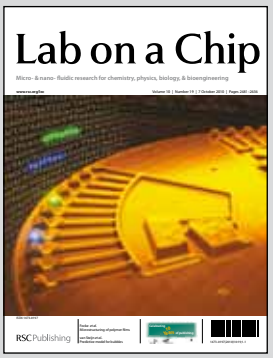

See Volkert van Steijn, Chris R. Kleijn and Michiel T. Kreutzer,
Lab Chip, 2010, **10**, 2513.

Predictive model for the size of bubbles and droplets created in microfluidic T-junctions

Volkert van Steijn,*[a] Chris R. Kleijn[a] and Michiel T. Kreutzer[b]

Received 8th February 2010, Accepted 16th June 2010
DOI: 10.1039/c002625e

We present a closed-form expression that allows the reader to predict the size of bubbles and droplets created in T-junctions without fitting. Despite the wide use of microfluidic devices to create bubbles and droplets, a physically sound expression for the size of bubbles and droplets, key in many applications, did not yet exist. The theoretical foundation of our expression comprises three main ingredients: continuity, geometrics and recently gained understanding of the mechanism which leads to pinch-off. Our simple theoretical model explains why the size of bubbles and droplets strongly depends on the shape of a T-junction, and teaches how the shape can be tuned to obtain the desired size. We successfully validated our model experimentally by analyzing the formation of gas bubbles, as well as liquid droplets, in T-junctions with a wide variety of shapes under conditions typical to multiphase microfluidics.

Introduction

Bubbles and droplets of microscopic size are indispensible in a broad range of applications, such as in bio-chemical and material synthesis, drug discovery and medical diagnostics and treatments.[1] In almost all applications, the size of bubbles and droplets needs to be known precisely. The need to predict this size in designing microfluidic devices is what motivated our work.

The success of microfluidic bubble and droplet generators is explained by their ability to reproducibly form equal-sized bubbles and droplets at high-throughput. The most popular generators[2] are based on hydrodynamic flow focusing,[3] co-flowing[4] and cross-flowing.[5]

[a]*Prins Bernhardlaan 6, NL-2628 BW Delft, The Netherlands. E-mail: V.vansteijn@tudelft.nl; C.R.Kleijn@tudelft.nl; Fax: +31 15 278 2838; Tel: +31 15 278 2839*
[b]*Julianalaan 136, NL-2628 BL Delft, The Netherlands. E-mail: M.T.Kreutzer@tudelft.nl; Fax: +31 15 278 5006; Tel: +31 15 278 9084*

In this work, we consider the formation of bubbles and droplets at T-junctions. Under circumstances typical to multiphase microfluidics—fluid streams confined by the geometry of the channels, and interfacial forces dominating over viscous, inertial and gravitational forces—bubbles (or droplets) form as displayed in Fig. 1. A formation cycle starts with a *filling period* in which the gas stream—injected from the side channel—penetrates into the stream of liquid. Liquid can freely flow around the erupting bubble until the bubble approaches the wall opposite to the side channel, which marks the start of the *squeezing period*. The bubble—its shape set by the geometry of the junction—now almost fully obstructs the liquid stream, confining it to the small regions in between the bubble and walls. Instead of flowing around the bubble, a large fraction of the incoming liquid pushes the bubble downstream with a velocity comparable to the average velocity of the liquid until pinch-off occurs. Garstecki *et al.*[6] showed that the size of bubbles and droplets at the end of the filling period V_{fill} is roughly independent of flow conditions, while the volume added to bubbles and droplets during the squeezing period linearly scales with the ratio of flow rates of the

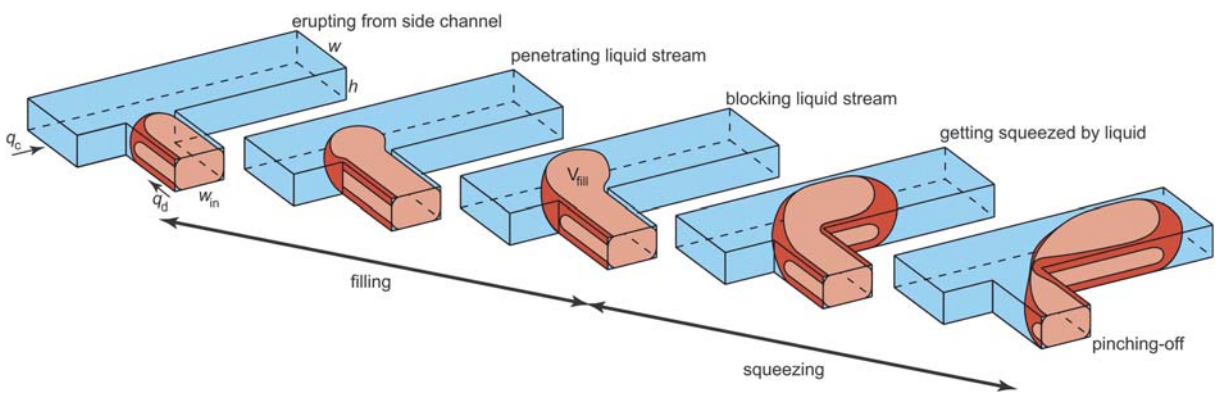

Fig. 1 Formation of a bubble at a planar T-junction with height h. Liquid and gas, respectively, enter the main channel (width: w) and side channel (width: w_{in}) at rates of flow q_c and q_d. A formation cycle comprises two periods: a filling period in which the bubble fills-up the junction and grows to a size V_{fill} and a squeezing period in which the forming bubble is squeezed by the liquid until it pinches-off.

dispersed and continuous phase q_d/q_c. Hence, the final volume V of a bubble or droplet—normalized with hw^2—is

$$\frac{V}{hw^2} = \frac{V_{fill}}{hw^2} + \alpha\frac{q_d}{q_c} \quad (1)$$

To predict the size of bubbles and droplets, one needs the value of the parameters V_{fill} and α. As closed-form expressions for these parameters are not available, V_{fill} and α are often treated as fitting parameters and determined empirically for a specific device.[7] A superior methodology to determine them would be to understand how they depend on the geometry of a T-junction.

In this paper, we present expressions for V_{fill} and α derived from simple theoretical arguments, which predict bubble and droplet size for a given geometry of a T-junction. For the reader who is mainly interested in the final result, we structured the paper such that we directly provide these expressions. Following that, we present all the theoretical foundations and the experimental validation.

Essential to the success of bubble and droplet-based microfluidic platforms is the ability to control the size of bubbles and droplets without changing the rates of flow. Recently, several methods have been explored to achieve this independent control, for instance using magnetic, electric, centrifugal and thermal forces.[8] Our contribution points out that controlling the geometry of a junction is an effective way to control the size of bubbles and droplets for given flow rates.[9] Moreover, it teaches how to change the geometry to obtain the desired size.

Summary of main results

The dimensionless volume of a bubble or droplet V/hw^2 is calculated as the sum of the dimensionless volumes V_{fill}/hw^2 and $\alpha q_d/q_c$ injected during the filling and squeezing period respectively. The dimensionless volume V_{fill}/hw^2 can be calculated with the two equations displayed in the top left part of Fig. 2: the first expression holds in case the width of the side channel is smaller than the width of the main channel ($w_{in} \leq w$), while the second relation should be used in case $w_{in} > w$. How to calculate α is displayed in the top right part of Fig. 2.

Note that V_{fill}/hw^2 and α are both fully characterized by h/w, w_{in}/w and ε/w, the three parameters that define the shape of a T-junction (see Fig. 4). We plotted V_{fill}/hw^2 and α as a function of h/w for several values of w_{in}/w, for sharp-edged T-junctions ($\varepsilon = 0$) in the bottom left and right parts of Fig. 2, respectively. These graphs show that the dimensionless volume V_{fill}/hw^2 moderately depends on the shape of a junction, while α moderately depends on h/w and strongly depends on w_{in}/w.

Comparison with experiments

We validated our theoretical model using experiments for junctions with $0.33 \leq w_{in}/w \leq 3$ and $0.1 \leq h/w \leq 0.5$ under the conditions that the capillary number Ca—a dimensionless number expressing the relative importance between viscous and capillary forces and defined as $Ca = \mu U/\gamma$ with U and μ the average velocity and viscosity of the continuous phase, respectively, and γ the interfacial tension—is smaller than 0.01.

The quality of our model is illustrated from a comparison of the sizes of bubbles and droplets predicted by our model and those measured in our experiments. We plotted the dimensionless volume of bubbles against the ratio of flow rates for five T-junction geometries in Fig. 3. In addition, one set of validating experiments is shown for liquid droplets. The experiments all

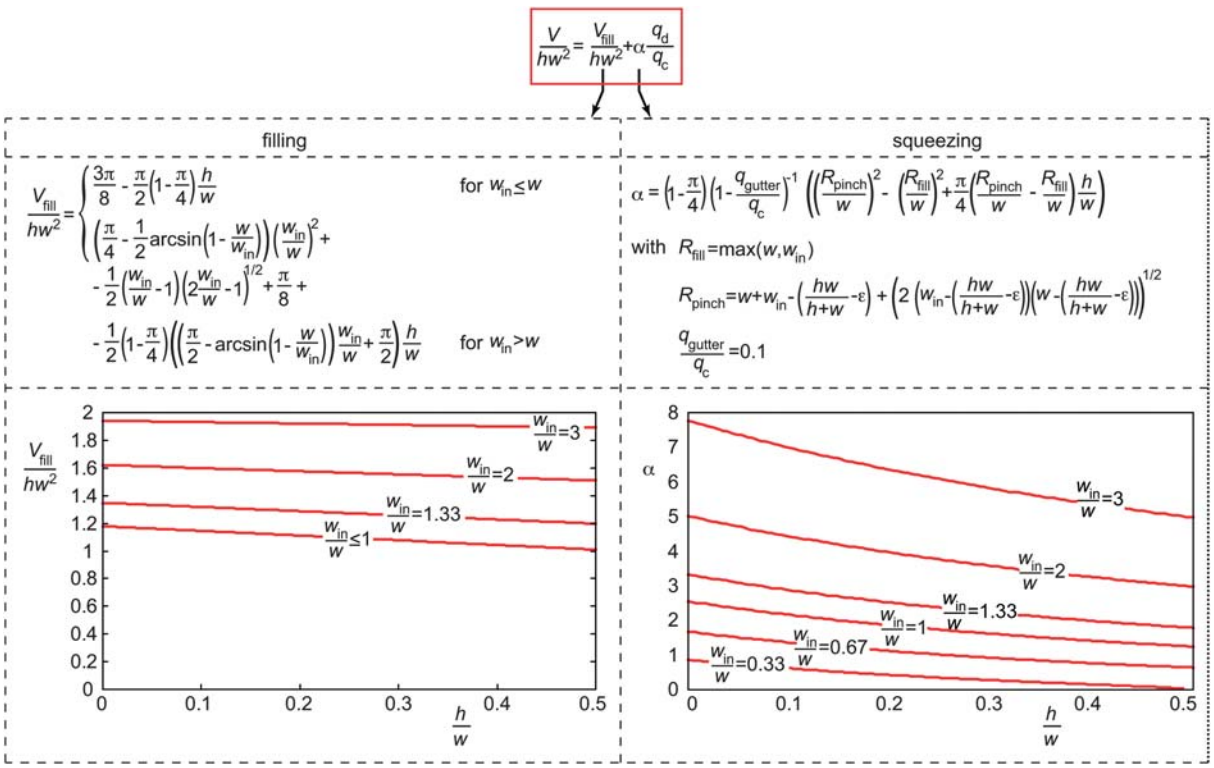

Fig. 2 Expressions in the top part allow the reader to calculate the final size of bubbles and droplets for a given T-junction geometry. The graphs in the bottom part show how the expressions for V_{fill}/hw^2 and α depend on the shape of a T-junction characterized by h/w and w_{in}/w for $\varepsilon = 0$.

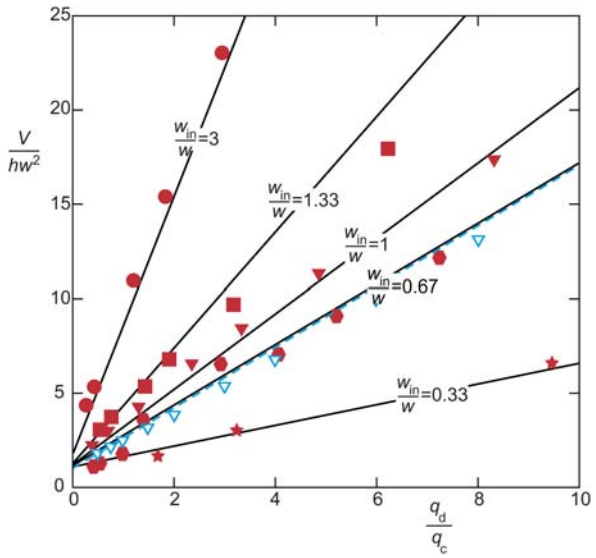

Fig. 3 The dimensionless volume of bubbles and droplets plotted against the ratio of flow rates q_d/q_c. For a given ratio of flow rates, the volume strongly depends on w_{in}/w. Our model (solid lines for gas–liquid and dashed line for liquid–liquid) shows good agreement with our gas–liquid measurements (filled symbols) and liquid–liquid measurement (open symbols). Geometries: (w_{in}/w, h/w) = (0.33, 0.33), (0.67, 0.11), (1, 0.33), (1.33, 0.17) and (3, 0.33); $\varepsilon = 0.1w$ for gas bubbles and (w_{in}/w, h/w) = (1, 0.48); and $\varepsilon = 0.01w$ for liquid droplets.

confirm the linear relation between V/hw^2 and q_d/q_c for a given geometry. Moreover, they confirm that the size of bubbles and droplets strongly depends on geometry: for instance, bubbles created at a junction with $w_{in}/w = 3$ are roughly ten times larger than those created at a junction with $w_{in}/w = 0.33$ for given ratios q_d/q_c and h/w. The main conclusion drawn from Fig. 3 is that our model is in good agreement with our experiments.

Model for bubble and droplet formation

Our model describes the formation of non-wetting bubbles and droplets in *confined* T-junctions with interfacial forces dominating over viscous forces and a negligible influence of inertial and gravitational forces. Under these circumstances, often referred to as the *squeezing regime*, bubbles and droplets grow so large that they obstruct the stream of the continuous phase thereby touching the four walls of the main channel as sketched in Fig. 1. This regime is encountered for Ca < 0.01 (10) and not too small values of w_{in}/w for shallow junctions commonly integrated in multiphase microfluidic platforms. For large Ca, or small w_{in}/w, the formation mechanism is different from that studied here: bubbles and droplets are sheared-off from the side feed channel before they obstruct the stream of the continuous phase and get squeezed.[10]

An important consequence of confinement is that the interface of bubbles and droplets growing in confined geometries is stable against small perturbations, which is not the case in unconfined geometries.[11] The shape of bubbles and droplets in such junctions is imposed by the geometry and, for low Ca, deformation of the interface due to viscous shear is negligible. The interface is in a quasi-equilibrium during almost the entire formation cycle with a minimum in surface energy.

One main ingredient in our model is the geometrical description of the shape of a bubble or droplet. For the sake of simplicity, we geometrically reconstruct the three-dimensional (3-D) shape from two-dimensional (2-D) views. The interface of a 2-D non-wetting bubble or droplet—which has a minimum in surface energy during its growth in a confined geometry at low Ca—takes the shape of a circle segment tangential to the walls in the regions where it is not touching the walls. At the front of the bubble or droplet, the 2-D shape is imposed by the width of the main channel and described with half a circle with radius $w/2$. At the rear, the shape is imposed by both the side and the main channel and described with a quarter of a circle with radius R as displayed in the bottom left of Fig. 4. Based on this 2-D top-view image, we reconstruct the 3-D shape by extrusion, hereby taking into account the curvature of the interface. We describe the shape of the interface in the third dimension with half a circle that fits in between the top and bottom wall and has a radius $h/2$ as shown in the bottom right of Fig. 4. In this way, calculation of a volume from a 2-D shape is straightforward. The volume of a fluid compartment relates to its 2-D top-view area A and perimeter l as

$$V = hA \pm 2\left(\frac{h}{2}\right)^2\left(1 - \frac{\pi}{4}\right)l \qquad (2)$$

The second term on the right hand side accounts for the volume of the continuous phase in-between the interface at the

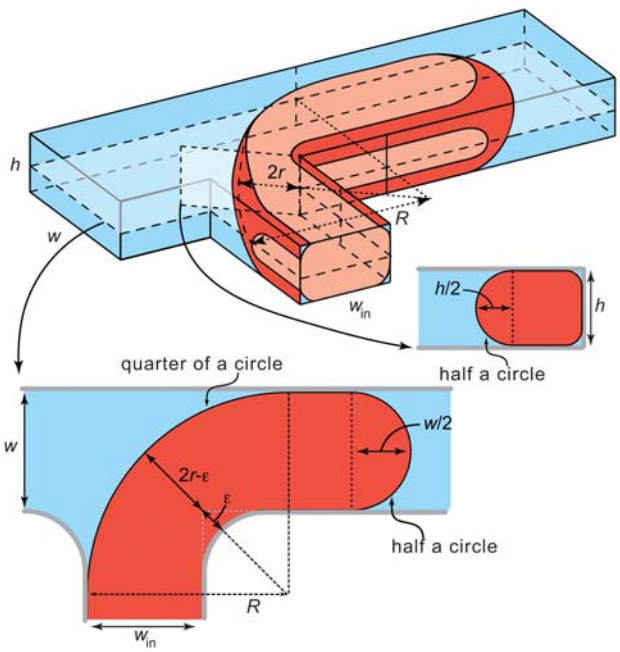

Fig. 4 Simple geometrical reconstruction used to calculate the size of a bubble or droplet using two-dimensional views. The top-view image shown on the bottom left shows that the receding interface takes the shape of a quarter of a circle with radius R, while the front of the bubble is described with half a circle with radius $w/2$. The rounded corners of the T-junction are characterized by the distance ε. We extend this 2-D picture into the third dimension by extrusion, hereby taking into account the curvature of the interface as shown on the bottom right. This curvature is again described with half a circle now with radius $h/2$.

midplane of the junction and the top and bottom walls, along the perimeter of the interface. The plus sign in this equation should be used for a compartment of the continuous phase, and the minus sign for a compartment of the dispersed phase.

In the following, we use the geometric description in combination with continuity arguments and recently gained understanding of the mechanism that triggers bubble pinch-off[12] to derive the expressions for V_{fill}, R_{fill}, α, and R_{pinch} presented in Fig. 2.

Filling

We describe the 2-D shape of a bubble or droplet at the end of the filling period with a quarter of a circle with radius R_{fill} at the rear, connected to half a circle with radius $w/2$ at the front as shown in Fig. 5. The receding interface is either constrained by the side or the main channel, which leads to the simple description for the radius $R_{fill} = \max(w_{in},w)$.

The derivation of the relations for V_{fill}—presented in Fig. 2—is straightforward and done by calculating the areas shown in Fig. 5 together with the perimeters and subsequently substituting them in eqn (2).

Squeezing

We now consider the squeezing period. We derive the analytical expression for α by calculating the volume $\alpha h w^2 q_d/q_c$ supplied to the bubble or droplet during this period. Continuity dictates that this volume equals the flow rate of the dispersed phase—supplied at a fixed rate q_d—integrated over the duration of the squeezing period $\Delta t_{squeeze}$. Hence,

$$\alpha h w^2 \frac{q_d}{q_c} = \Delta t_{squeeze} q_d \tag{3}$$

The squeezing period is the time it takes for the continuous phase to push the bubble or droplet from its position at the end of the filling period in downstream direction until pinch-off takes place. The rate-of-change in volume dV_c/dt associated with this displacement is given by a second continuity argument, now for the continuous phase, and relates to the flow rate of the continuous phase supplied at a fixed rate q_c as

$$\frac{dV_c}{dt} = q_c\left(1 - \frac{q_{gutter}}{q_c}\right) \tag{4}$$

with q_{gutter}/q_c the fraction of the flow rate of the continuous phase that—instead of pushing the bubble or droplet downstream—bypasses the bubble or droplet and flows along the corners of the main channel, which are not invaded by the bubble or droplet. We refer to these regions as gutters.

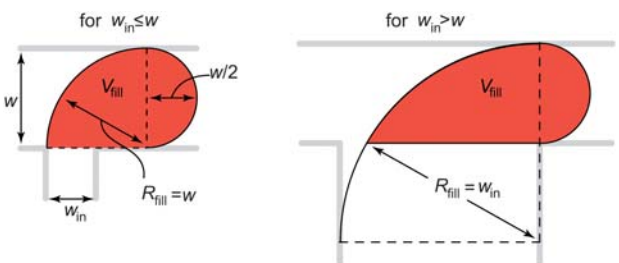

Fig. 5 Shape of a bubble or droplet at the end of the filling period in case $w_{in} \le w$ (left) and $w_{in} > w$ (right).

We express dV_c/dt in terms of R using our simple geometric description of the shape of a bubble or droplet. The change in the area δA_c behind the receding interface relates to the change in radius δR as $\delta A_c = (1 - \pi/4)\delta R^2$. Similarly, for the change in the perimeter δl of the receding interface, we find $\delta l = (\pi/2)\delta R$. Substitution of these expressions in eqn (2) results in an expression for dV_c/dt in terms of R. Substitution of this expression in eqn (4) results in an equation that describes the dynamics of the interface

$$\left[2\frac{R}{w} + \frac{\pi}{4}\frac{h}{w}\right]\frac{d}{dt}\left(\frac{R}{w}\right) = \frac{q_c}{hw^2}\left(1 - \frac{\pi}{4}\right)^{-1}\left(1 - \frac{q_{gutter}}{q_c}\right) \tag{5}$$

The evolution of the radius R is found by integration of this equation. Integration over the duration of the squeezing period yields an expression for the squeezing period

$$\Delta t_{squeeze} = \left(1 - \frac{\pi}{4}\right)\left(1 - \frac{\bar{q}_{gutter}}{q_c}\right)^{-1} \times \left[\left(\frac{R_{pinch}}{w}\right)^2 - \left(\frac{R_{fill}}{w}\right)^2 + \frac{\pi}{4}\frac{h}{w}\left(\frac{R_{pinch}}{w} - \frac{R_{fill}}{w}\right)\right]\frac{hw^2}{q_c} \tag{6}$$

with $\bar{q}_{gutter}$ the time-averaged flow rate through the gutters and R_{fill} and R_{pinch} the radii of the receding interface at the start and end of the squeezing period. Based on previous work,[12,13] we use $q_{gutter}/q_c = 0.1$ throughout this paper. The expression for α presented in Fig. 2 is obtained by substitution of $\Delta t_{squeeze}$ in eqn (3). Finally, we derive an expression for R_{pinch}.

Radius R_{pinch} at pinch-off

Remarkably, a bubble or droplet pinches-off before the receding interface collapses at the sidewalls of a T-junction. Previously,[12] we have shown that the gas thread that connects a forming bubble to the side feed rapidly collapses as soon as the pressure inside the liquid upstream of the receding interface $p_{L,rear}$ becomes smaller than the pressure inside the liquid downstream of the nose of the bubble $p_{L,front}$. In brief, the pressure difference over the forming bubble or droplet can be calculated using the static Laplace pressure jumps at the rear and front of the bubble or droplet. Prior to pinch-off, these pressure jumps over the interface are $p_d - p_{L,rear} = \gamma(1/R + 1/r)$ and $p_d - p_{L,front} = \gamma(2/h + 2/w)$, respectively, with the radii r and R as defined in Fig. 4. Taking the pressure inside the bubble or droplet p_d uniform, the pressure difference $p_{L,rear} - p_{L,front}$ becomes negative once the radius r equals

$$2r_{pinch} = \frac{hw}{h + w} \tag{7}$$

where we neglected the curvature $1/R$ with respect to $1/r$. This criterion shows that bubbles and droplets pinch-off at a geometry-dependent moment. The expression for R_{pinch} presented in Fig. 2 is obtained by reworking this criterion in terms of R using the relation between $2r$ and R

$$2r - \varepsilon = R - \sqrt{(R - w)^2 + (R - w_{in})^2} \tag{8}$$

This relation is purely based on geometrics as illustrated in the top left sketch in Fig. 4. The distance ε—exaggerated for

clarity—characterizes the rounded corners of our T-junctions. We stress here that it is important to take the roundness of the corners into account, because the size of bubbles and droplets is quite sensitive to ε as illustrated by the following example: neglecting a rounded corner of $\varepsilon \approx 0.1w$ for a T-junction with $h/w = 0.33$ and $w_{in}/w = 1$ results in an underestimation of α by more than 15%.

Gas bubbles *versus* liquid droplets

Up to now, we did not discuss the influence of fluid properties. Garstecki *et al.*[6] explained from an order of magnitude analysis that the forces dominating the formation of a bubble or droplet are insensitive to the viscosity and density of the continuous and dispersed phase. Their conclusion that the size of bubbles and droplets can be predicted with the same equation was supported by gas–liquid and liquid–liquid experiments. In line with their findings, the main ingredients of our model are independent of fluid properties, and our model can both be used to predict the size of gas bubbles and liquid droplets as evident from Fig. 3.

Experimental

We used a high-speed camera attached to an inverted microscope to record the formation of bubbles and droplets in T-junctions with a wide variety of shapes, *i.e.* $w_{in}/w = 0.33$–3 and $h/w = 0.1$–0.5, the width of the main channel hereby in the range $w = 100$–300 μm.

In our gas–liquid experiments, air and ethanol ($\mu = 1.2$ mPa s and $\gamma = 22.7$ mN m^{-1}) were used as the dispersed and continuous phase respectively. No surfactants were added. In our liquid–liquid experiments, we dispersed demineralized water in a 10% solution of perfluorooctanol (PFO) in perfluorodecalin (PFD) ($\mu = 7.2$ mPa s). The interfacial tension at the liquid–liquid interface was measured as $\gamma = 17.9$ mN m^{-1}. Syringe pumps were used to drive the liquids into the device, with flow rates in the range 1–32 μL min^{-1}. A steady flow of gas, injected at a rate in the range 9–40 μL min^{-1}, was controlled using a needle valve connected to a 2 m long capillary tube with internal diameter of 100 μm that stabilized the flow. The capillary number based on the average velocity of the continuous phase, $Ca = \mu q_c/\gamma wh$, was below 0.01 in all our experiments.

Devices were fabricated using soft lithography. Poly(dimethylsiloxane) (PDMS) slabs containing the fluidic networks were sealed to glass slides for our gas–liquid experiments and to glass slides coated with a thin layer of PDMS in our liquid–liquid experiments. The air plasma treatment used to seal the devices renders the surface of PDMS hydrophilic. After exposure, the static contact angle of ethanol on PDMS and glass is $\theta_e < 10°$. For our gas–liquid experiments, we used the devices immediately after the plasma treatment to prevent recovery of the hydrophobicity. To also obtain almost complete wetting in our liquid–liquid experiments, we functionalized the microchannel walls as follows. After plasma bonding, we allowed hydrophobic recovery of PDMS, and baked the channels in the oven at 68 °C for 24 h. We then flowed a 5% solution of 1*H*,1*H*,2*H*,2*H*-perfluorooctyltrichlorosilane in ethanol through the channels at a rate of 5 μL min^{-1} for 30 min, followed by flowing a 100% ethanol stream at a rate of 10 μL min^{-1} for 30 min. Before use, the channels were flushed with air and baked in the oven at 68 °C for 12 h. The contact angle of a droplet of water on a functionalized PDMS surface immersed in the 10% solution of PFO in PFD was measured to be $\theta_e \approx 10°$.

The distance ε characterizes the rounding of the corners of our microfabricated T-junction as shown in Fig. 4. We measured ε for each device, with $\varepsilon \approx 0.1w$. We used the value for ε in the calculation of the theoretical results plotted in Fig. 3 and Fig. 6b.

The bubble and droplet volumes shown in Fig. 3 were extracted from our micrographs as follows: after the release of a bubble or a droplet from the T-junction, the length L (cap-to-cap) was measured and used in combination with eqn (2) to derive the volume. We hereby described the 2-D shapes of bubbles and droplets with two half circles connected with a rectangle such that the area and perimeter of a bubble or droplet are $A = \pi(w/2)^2 + w(L - w)$ and $l = \pi w + 2(L - w)$. Of course, more sophisticated geometric reconstructions can be used to derive the volume of a bubble or droplet from its length, but that is beyond the point here. The values shown in Fig. 3 represent the average over sets of typically more than 100 bubbles or droplets. The standard deviation in the length was typically less than 3%. In our gas–liquid experiments, the gas flow rate was calculated by multiplying the bubble volume V with the bubble formation frequency measured from our micrographs.

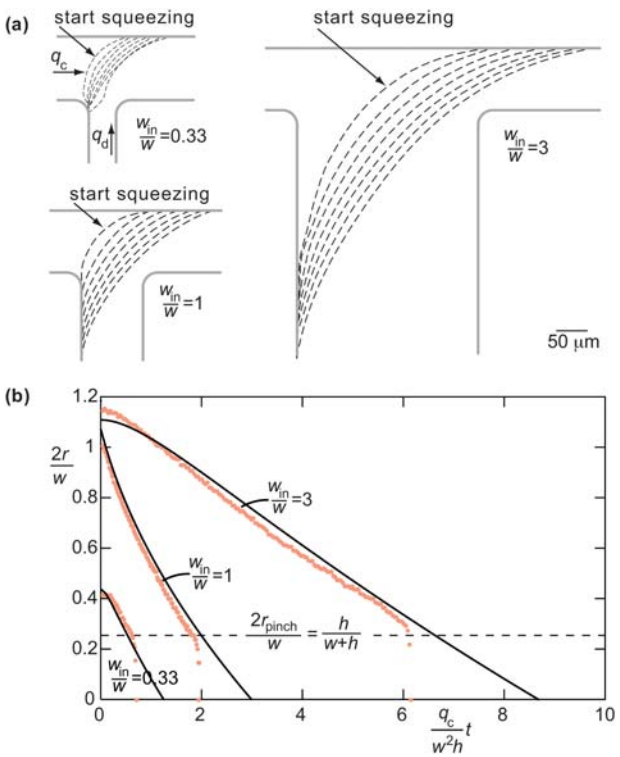

Fig. 6 Evolution of the receding interface during the squeezing period for three junctions with $w_{in}/w = 0.33$, 1 and 3. (a) Interface profiles extracted from micrographs are equidistant in time and show the receding interface taking the shape of a quarter of a circle. (b) The evolution of the distance $2r$ predicted with our model (solid lines) agrees well with the measurements, with the criterion $2r/w = h/(h + w)$ (dashed line) accurately predicting when pinch-off takes place ($h = 33$ μm, $w = 100$ μm, $\varepsilon = 0.1w$, and $q_c = 3$ μL min^{-1}).

Validation of theoretical model from experiments

The first key ingredient of our model is the geometric description of the receding interface with a quarter of a circle during the squeezing period. We present experimentally observed profiles of the receding interface—equidistant in time—for junctions with $w_{in}/w = 0.33$, 1, and 3 in Fig. 6a. These profiles show qualitatively that our description of the interface with a quarter of a circle is physically sound.

The second key ingredient of our model is the continuity argument used to derive the dynamics of the receding interface during the squeezing period. We show the evolution of the interface by plotting the shortest distance between interface and junction $2r$ normalized with w as a function of time t normalized with q_c/hw^2 in Fig. 6b. Our model is in good quantitative agreement with our measurements. The solid lines representing our model were obtained from integration of eqn (5) and reworking the result in terms of r using eqn (8).

The third key ingredient was inferred from the mechanism of pinch-off and tells us that pinch-off takes place as soon as $2r$ becomes smaller than $wh/(w + h)$. Fig. 6b shows that the distance $2r$—initially decreasing at an almost linear rate—rapidly decreases towards zero once this criterion is met. Although only shown for our gas–liquid experiments in Fig. 6b, this criterion was found to be equally valid for our liquid–liquid measurements. We stress here that not taking into account this criterion leads to a significant over prediction of the squeezing period and hence of α. For $h/w = 0.33$, α would be over predicted by roughly a factor of 1.5. This becomes evident when comparing the squeezing period found in our experiments with the one predicted by our model in case we ignore the criterion and extrapolate the theoretical curves describing the evolution until they cross the horizontal axis as shown in Fig. 6b.

Conclusion and discussion

We have presented a physically sound expression that allows the reader to predict the size of bubbles and droplets formed at microfluidic T-junctions under conditions typical to multiphase microfluidic platforms. The strong dependence of bubble and droplet size on the shape of the junction follows in an insightful way from the expression, which makes it a relevant extension of the scaling rule by Garstecki *et al.*[6] Our model has been experimentally validated for gas bubbles, as well as for liquid droplets, formed in T-junctions with $0.33 \leq w_{in}/w \leq 3$ and $0.1 \leq h/w \leq 0.5$ for $Ca < 0.01$. Good agreement was found between our model and our experiments. We expect that the methodology put forward in this paper can be successfully applied to other types of geometries as well.

References

1 S.-Y. Teh, R. Lin, L.-H. Hung and A. P. Lee, *Lab Chip*, 2008, **8**, 198–220; A. Huebner, S. Sharma, M. Srisa-Art, F. Hollfelder, J. B. Edel and A. J. deMello, *Lab Chip*, 2008, **8**, 1244–1254.

2 G. F. Christopher and S. L. Anna, *J. Phys. D: Appl. Phys.*, 2007, **40**, R319–R336.

3 A. M. Gañán-Calvo and J. M. Gordillo, *Phys. Rev. Lett.*, 2001, **87**, 274501; S. L. Anna, N. Bountoux and H. A. Stone, *Appl. Phys. Lett.*, 2003, **82**, 364.

4 P. B. Umbanhowar, V. Prasad and D. A. Weitz, *Langmuir*, 2000, **16**, 347–351.

5 T. Thorsen, R. W. Roberts, F. H. Arnolds and S. R. Quake, *Phys. Rev. Lett.*, 2001, **86**, 4163–4166.

6 P. Garstecki, M. J. Fuerstman, H. A. Stone and G. M. Whitesides, *Lab Chip*, 2006, **6**, 437–446.

7 A. R. Abate, A. Poitzsch, Y. Hwang, J. Lee, J. Czerwinska and D. A. Weitz, *Phys. Rev. E: Stat. Phys., Plasmas, Fluids, Relat. Interdiscip. Top.*, 2009, **80**, 026310; D. M. Fries and P. R. von Rohr, *Microfluid. Nanofluid.*, 2009, **6**, 27–35.

8 C. N. Baroud, J.-P. Deville, F. Gallaire and R. Wunenburger, *Phys. Rev. E: Stat. Phys., Plasmas, Fluids, Relat. Interdiscip. Top.*, 2007, **75**, 046302; C.-W. Chang, Y.-T. Cheng, C.-Y. Tsai, J.-H. Chien, P.-Y. Wang and P.-H. Chen, *J. Magn. Magn. Mater.*, 2007, **310**, 2844–2846; S. Haeberle, R. Zengerle and J. Ducrée, *Microfluid. Nanofluid.*, 2007, **3**, 65–75; D. R. Link, E. Grasland-Mongrain, A. Duri, F. Sarrazin, Z. Cheng, G. Cristobal, M. Marquez and D. A. Weitz, *Angew. Chem., Int. Ed.*, 2006, **45**, 2556–2560; F. Malloggi, S. A. Vanapalli, H. Gu, D. van den Ende and F. Mugele, *J. Phys.: Condens. Matter*, 2007, **19**, 462101; N.-T. Nguyen, T.-H. Ting, Y.-F. Yap, T. N. Wong, J. C.-K. Chai, W.-L. Ong, J. Zhou, S.-H. Tan and L. Yobas, *Appl. Phys. Lett.*, 2007, **91**, 084102; C. A. Stan, S. K. Y. Tang and G. M. Whitesides, *Anal. Chem.*, 2009, **81**, 2399–2402.

9 A. R. Abate, M. B. Romanowsky, J. J. Agresti and D. A. Weitz, *Appl. Phys. Lett.*, 2009, **94**, 023503; C.-Y. Lee, Y.-H. Lin and G.-B. Lee, *Microfluid. Nanofluid.*, 2009, **6**, 599–610.

10 G. F. Christopher, N. N. Noharuddin, J. A. Taylor and S. L. Anna, *Phys. Rev. E: Stat. Phys., Plasmas, Fluids, Relat. Interdiscip. Top.*, 2008, **78**, 036317; M. de Menech, P. Garstecki, F. Jousse and H. A. Stone, *J. Fluid Mech.*, 2008, **595**, 141–161.

11 P. Garstecki, H. A. Stone and G. M. Whitesides, *Phys. Rev. Lett.*, 2005, **94**, 164501; P. Guillot, A. Colin and A. Ajdari, *Phys. Rev. E: Stat. Phys., Plasmas, Fluids, Relat. Interdiscip. Top.*, 2008, **78**, 016307.

12 V. van Steijn, C. R. Kleijn and M. T. Kreutzer, *Phys. Rev. Lett.*, 2009, **103**, 214501.

13 V. van Steijn, M. T. Kreutzer and C. R. Kleijn, *Chem. Eng. Sci.*, 2007, **62**, 7505–7514.

